Technical note

Stochastic analysis of a heterogeneous micro-finite element model of a mouse tibia

Yongtao Lu [a,b], Di Zuo [b], Junyan Li [c], Yiqian He [a,b,*]

[a] State Key Laboratory of Structural Analysis for Industrial Equipment, Dalian University of Technology, No. 2 Linggong Road, Dalian, 116024, China
[b] Department of Engineering Mechanics, Dalian University of Technology, No. 2 Linggong Road, Dalian, 116024, China
[c] Department of Design Engineering and Mathematics, School of Science and Technology, Middlesex University, The Burroughs, Hendon, London NW4 4BT, UK

ARTICLE INFO

ABSTRACT

Finite element (FE) analysis can be used to predict bone mechanical environments that can be used for many important applications, such as the understanding of bone mechano-regulation mechanisms. However, when defining the FE models, uncertainty in bone material properties may lead to marked variations in the predicted mechanical environment. The aim of this study is to investigate the influence of uncertainty in bone material property on the mechanical environment of bone.

A heterogeneous FE model of a mouse tibia was created from micro computed tomography images. Axial compression loading was applied, and all possible bone density-modulus relationships were considered through stochastic analysis. The 1st and 3rd principal strains (ε_1 and ε_3) and the strain energy density (SED) were quantified in the tibial volume of interest (VOI).

The bounds of ε_1, ε_3, and SED were determined by the bounds of the density-modulus relationship; the bone mechanical environment (ε_1, ε_3, and SED) and the bone density-modulus relationship exhibit the same trend of change; the relative percentage differences caused by bone material uncertainty are up to 28%, 28%, and 21% for ε_1, ε_3, and SED, respectively. These data provide guidelines on the adoption of bone density-modulus relationship in heterogeneous FE models.

© 2018 IPEM. Published by Elsevier Ltd. All rights reserved.

1. Introduction

Micro computed tomography (μCT) imaging has become an important tool to reveal the detailed internal structure of bone, both ex vivo and in vivo [1,2]. μCT images can be used to generate micro-finite element (μFE) models, in which the element size is on the order of micrometers, to investigate the mechanical behavior of bone, the mechanism of bone mechano-regulation, and the strength of bone after medical intervention [3–8]. Because the homogeneous μFE models lack realistic spatial variations in bone properties and exhibit limited accuracy, heterogeneous μFE models with heterogeneous material properties have been adopted widely in previous studies [9–11].

To generate heterogeneous μFE models of the bone from μCT images, the raw CT attenuation values must first be related to the bone mineral density (BMD) and subsequently converted to bone material properties using bone density-modulus relationship. The

relationship between CT attenuation values and BMD values can be established by first scanning the calibration phantom that contains several rods with known BMD values provided by the manufacturer, and subsequently fitting a linear line to the scatter data of the CT attenuation and BMD values of the rods [12]. The bone density-modulus relationship is typically obtained by first performing a mechanical testing on the bone samples at the organ-level and subsequently relating these bone mechanical properties to the various bone densities (apparent density, ash density, etc.) [13]. Because the mechanical properties obtained from mechanical testing are apparent values at the organ-level and the microstructures of bone varies significantly among samples, large variations occur in the bone density-modulus relationship [9–11,14]. It is still unclear how these variations affect the predictions of heterogeneous μFE models.

The detailed mechanical environment could provide important information for the full-field validation of bone FE models [15] and for understanding the mechanical signals driving bone adaptations [16]. For an example, it has been found that bone sites with high strain energy density (SED) exhibit more activities of bone formation; on the contrary, low SED leads to bone resorption [16,17]. However, the uncertainties in bone density-modulus relationships

* Corresponding author: State Key Laboratory of Structural Analysis for Industrial Equipment, Dalian University of Technology, No.2 Linggong Road, Dalian, 116024, China.
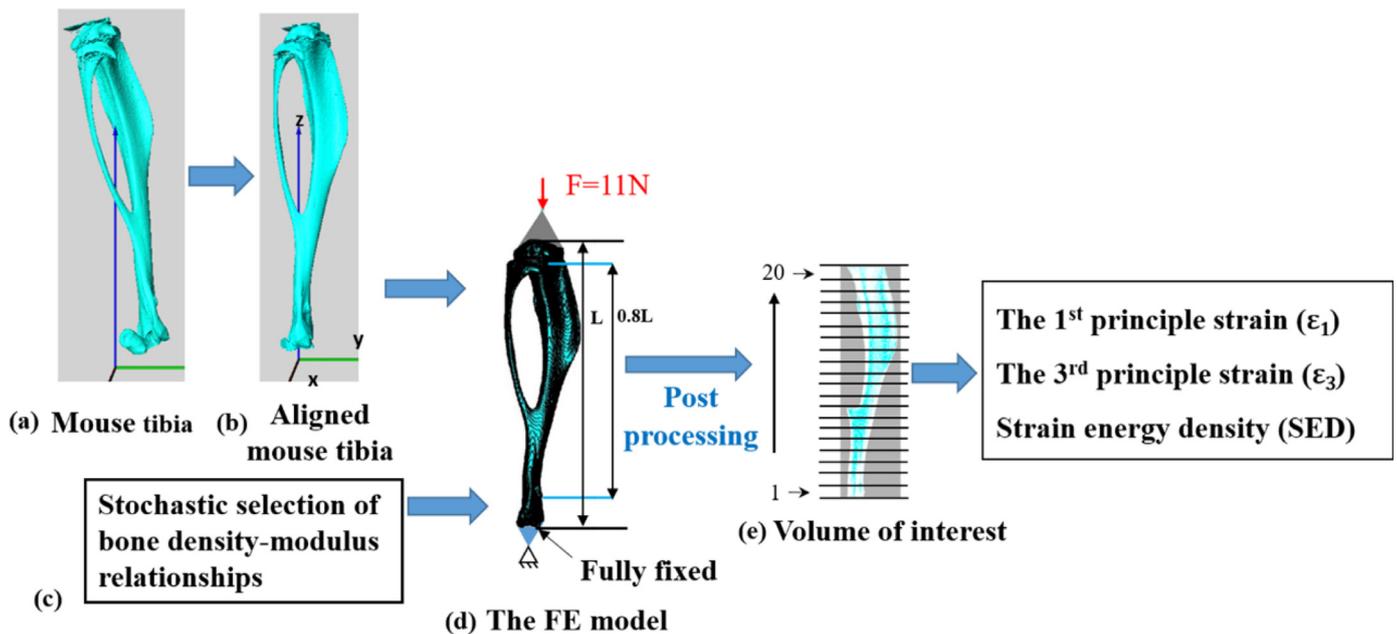
E-mail address: heyiqian@dlut.edu.cn (Y. He).

Fig. 1. Schematic description of the image processing procedure. (a) The mouse tibia; (b) the tibia was aligned along the global coordinate system; (c) and (d) the μFE tibial model and boundary conditions; (e) the volume of interest (VOI) was partitioned into 20 compartments and the mechanical environment of the bone was quantified in the 20 compartments.

may affect the mechanical environment predicted from FE models. To account for these uncertainties, many stochastic analyses have been performed to assess the effect of variability in material property on the mechanical environment predicted by FE models [18–21]. However, these studies focused on either the peak values of the mechanical properties (maximal principal strains, maximal principal stresses, etc.) or the apparent behavior (fracture force, hardness, etc.) of the bone samples. The influence of variability in material properties on the detailed mechanical environment (i.e., the distribution of the 1st and 3rd principal strains and the strain energy density) across the entire bone spatial space is still unknown.

The aim of this study is to investigate the influence of uncertainty in bone material property on the detailed mechanical environment of the bone using heterogeneous μFE models and stochastic analysis.

2. Materials and methods

2.1. μCT image of mouse tibia and image processing

One entire right tibia dissected from a 12-week-old female C57Bl/6 mouse was imaged using the ex vivo μCT imaging system (SkyScan 1172, Bruker, Belgium) with the following setting: a voltage of 49 kV, a tube current of 179 μA, an exposure time of 1180 ms, and an isotropic image voxel size of 4.3 μm. In preparation for generating the FE models, the image datasets were processed based on the standard procedure developed previously [22]. In brief, the tibia was returned to its anatomic position, i.e., its long (proximal-distal) axis was aligned along the z-axis approximately, and the y–z plane passed through the central line of the articular surfaces of the medial and lateral condyles (Fig. 1(a) and (b)). This step was to facilitate the application of the compressive loading along the long axis of the mouse tibia. The image dataset was subsequently transformed into the new position and resampled using the Lanczos kernel, which is a low-pass filter and considered to be the "best compromise" among several simple filters [23].

2.2. Generation of heterogeneous finite element models of mouse tibia

The heterogeneous μFE model of the mouse tibia was generated from the transformed μCT images (Fig. 1(b) and (d)). In brief, the grayscale image dataset was first smoothed with a Gaussian filter (convolution kernel [3 3 3], standard deviation = 0.65) and subsequently binarized into bone and background using a single threshold value, i.e., 25.5% of maximal grayscale value (approximately 420 mg HA/cm^3). However, the tibia cannot be segmented completely using only one threshold value, because the images includes other bones, such as the femur. Therefore, the tibia and fibula were further segmented from other bones manually (Amira 5.4.3, FEI Visualization Sciences Group, France). The tibial–fibula joint and the region of tibial proximal growth plate were manually filled to allow for load transmission. From the binarized tibia–fibula images, the μFE model with the element number of 1,944,774 was created by converting each bone voxel into an eight-node hexahedral element mesh with the element type SOLID185 using an in-house developed Matlab code (Matlab 2015a, The Mathworks, Inc. USA). The boundary condition was based on the experimental setup used for the in vivo loading of the mouse tibia [7], i.e., all the nodes on the concave articular surface of the distal tibia were coupled to a distal reference point (RP), which is constrained in all degrees of freedom; the FE nodes at the tibial plateau surface were coupled rigidly to a proximal RP, on which a load of -11 N was applied [7] (Fig. 1(c)). Poisson's ratio for all the materials was set to 0.3. The uncertainty of the bone's Young's modulus (E) was considered by selecting the bone density-modulus relationship stochastically, which was an input of the FE models (Fig. 1(c) and (d)). The details of this step are described as below.

2.3. Stochastic selection of the bone density-modulus relationship

The uncertainty in Young's modulus (E) of the μFE bone models was treated through a stochastic analysis. First, after matching the anatomic sites, six density-modulus relationships of the
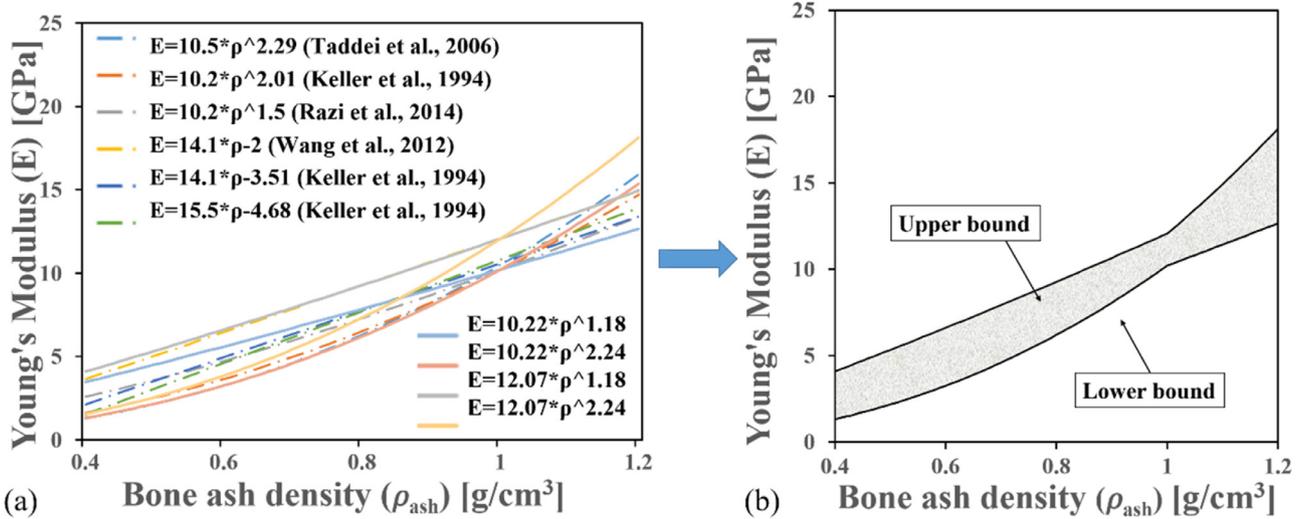
Fig. 2. Determination of the uncertain interval for the bone density-modulus relationships. (a) Fitting exponential functions to the density-modulus relationships available in the literature; (b) the determined bone density-modulus interval.

femur and tibia, which were typically adopted in the literature [13,14,24], were reviewed and plotted (Fig. 2(a)). Here, the data on other anatomic sites, such as the vertebra, were excluded, because these bones have markedly different structures compared to the tibia and femur.

Subsequently, exponential density-modulus relationships were fitted to the mechanical testing data of the bone samples by adjusting the constants "a" and "b" in the exponential function (Eq. (1)). Because the μFE model also included hollow structures of the bone (such as the tibia–fibula joint and the growth plate), which were generated by the manual filling of these regions in the image processing step, a lower threshold value of bone ash density of 0.4 g/cm^3 was adopted in the density-modulus relationship to avoid unrealistically low moduli in the μFE model. The modulus for the elements with bone ash density less than 0.4 g/cm^3 was set to 0.0104 MPa [13]. Meanwhile, some image voxels may have superficially high grayscale values owing to image noise, which lead to unrealistically high bone densities. Therefore, an upper threshold value of 1.2 g/cm^3 was defined in the density-modulus relationship [13]. In summary, the exponential density-modulus relationship used in this study was formulated as below:

$$E = \begin{cases} 0.0104 \times 10^{-3} & \rho_{ash} < 0.4 \\ a \times \rho_{ash}{}^{b} & 0.4 \leq \rho_{ash} \leq 1.2 \\ a \times 1.2^{b} & \rho_{ash} > 1.2 \end{cases} \quad (1)$$

where "a" and "b" are the two constants, E is Young's modulus (GPa), and ρ_{ash} is the bone ash density (g/cm^3). It is noteworthy that based on the conversion between bone apparent and ash densities [14], the relationship between bone apparent density and bone modulus can also be established and used for the investigations.

All possible bone moduli in the heterogeneous μFE models were considered by adjusting the two constants ("a" and "b" in Eq. (1)) within the range covered by the various bone density-modulus relationships reviewed (Fig. 2(a) and (b)). This was implemented and realized in two steps: first, the intervals of "a" and "b" were determined by initially selecting a relatively large interval and subsequently refined by optimizing the two constants by the simplex method (Fig. 2(b)) [25]; next, in the intervals calculated, "a" and "b" were selected stochastically based on the transformation method [26], which has been proven to reduce the computation cost effectively. It was found that when "a" changed

from 10.22 to 12.07 and "b" changed from 1.18 to 2.24, the exponential density-modulus function (Eq. (1)) covered the full uncertain interval of the bone density-modulus relationships reviewed (Fig. 2(b)).

2.4. Calibration of the bone modulus in the finite element models

For each stochastic selection of "a" and "b," the calcium hydroxyapatite (HA)-equivalent BMD was calculated at each μCT image voxel using the relationship established through scanning the calibration phantom. In the present study, the phantom with rod densities of 0.0 HA mg/cm^3, 250.0 HA mg/cm^3, and 750.0 HA mg/cm^3 was used. The phantom was scanned using the same setting as used for scanning the tibia. By calculating the image grayscale values at each rod of the phantom, the relationship of $\rho_{HA} = 0.0059 \times Igray + 0.242$ (ρ_{HA} is the HA-equivalent BMD, of units HA g/cm^3; $Igray$ is the image grayscale value) was established to convert the image grayscale values to HA-equivalent BMD values. After matching the phantom type and anatomic site, the density-conversion relationship of $\rho_{ash} = 0.877 \times \rho_{HA} + 0.079$ was chosen to convert the HA-equivalent BMD to bone ash density [14]. However, it is noteworthy that variability exists in this conversion and its influence on the bone mechanical environment requires further investigations. The modulus for each bone image voxel was calculated using Eq. (1) and subsequently mapped to the FE mesh using a Matlab code developed in-house.

2.5. Finite element analysis and post-processing

Based on the stochastic selection algorithm of the transformation method, 11 values were selected for both "a" and "b" in their intervals, thus resulting in 121 bone density-modulus relationships and 121 FE models. The FE models were solved using ANSYS (Release 14.0.3, ANSYS, Inc.) on a workstation (Intel Xeon E-5-2670. 2.60 GHz, 256 GB RAM) using the formulation of a linear elastic constitutive model.

To investigate the influence of uncertainty in bone material property on the mechanical environment of the mouse tibia, a volume of interest (VOI) was selected in the FE models. The VOI started from the end of the proximal growth plate and encompassed 80% of the tibial length (L), which was measured as the distance from the most proximal pixel of the mouse tibia until the most distal pixel of the mouse tibia, and is 17.82 mm for the
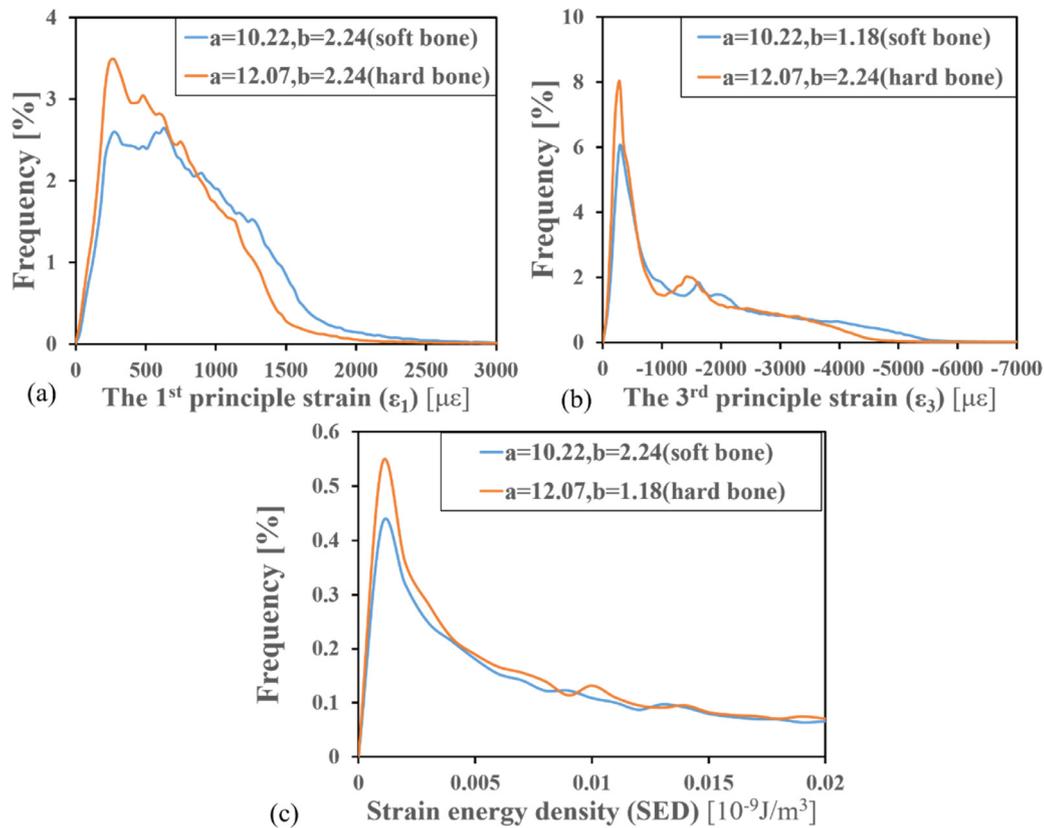
Fig. 3. The influence of material uncertainty on the occurrence frequency of the 1st principal strain, the 3rd principal strain, and the strain energy density. The plotted curves of occurrence frequency are the ones with the hardest and softest bone density-modulus relationships.

tibia analyzed in the present study (Fig. 1(d)). To quantify the results in the three-dimensional (3D) bone spatial space, the VOI was
partitioned into 20 compartments of equal length in the *z*-direction (Fig. 1(e)). Further, the normalized length of VOI was defined, with the value of zero at the distal end of the VOI. The 1st principal strain (ε_1), 3rd principal strain (ε_3), and SED were selected as the parameters to describe the mechanical environment of the mouse tibia (Fig. 1(e)), because ε_1 is likely linked to the bone opening fracture, ε_3 is the compressive strain reflecting the primary loading scenario in the bone, and SED is highly correlated with bone adaptations. The averaged values of ε_1, ε_3, and SED in the 20 compartments were calculated and plotted against the normalized VOI length. The post-processing of data in this manner is based on the previous findings where the mechanical values are not reproducible at the image voxel level, but are reliable over a larger VOI [22]. It was found that the bounds of ε_1, ε_3, and SED were determined by the upper and lower bounds of "a" and "b" and all different selections of "a" and "b" shared the same upper and lower bounds. Therefore, to determine the bounds of ε_1, ε_3, and SED, no further refinements on the selection of "a" and "b" were required.

3. Results

The occurrence frequencies corresponding to the softest and hardest bone material models are shown in Fig. 3. It was found that a lower bone stiffness led to higher ε_1, ε_3, and SED. Further, 86% of the nodes in the hardest bone model exhibit an ε_1 that is higher than 250 $\mu\varepsilon$ ($a = 12.07$, $b = 2.24$), compared to 89% of the nodes in the softest bone model ($a = 10.22$, $b = 2.24$). Meanwhile, 83% of the nodes in the hardest bone model exhibit an ε_3 lower

than $-250\,\mu\varepsilon$ ($a = 10.07$, $b = 2.24$), compared to 89% of the nodes in the softest bone model ($a = 10.22$, $b = 1.18$). In summary, if the softest bone model was used instead of the hardest bone model, 3% ($= 89\%$–86%) occurrence of ε_1 were shifted above 250 $\mu\varepsilon$ and 5% ($= 89\%$–83%) occurrence of ε_3 were shifted below $-250\,\mu\varepsilon$.

The material uncertainty-induced bounds of ε_1, ε_3, and SED across the tibial VOI are presented in Fig. 4. It was found that when the bone density-modulus relationship was changed in the FE models, the ε_1, ε_3, and SED across the tibial VOI exhibited the same trend of change (Fig. 4). A lower bone stiffness (soft bone) led to an increased ε_1, an increased SED and a decreased ε_3. It is noteworthy that the bounds of ε_1 and ε_3 were determined by different bone density-modulus relationships, i.e., the bounds of ε_1 were determined by $E = 10.22 \times \rho_{ash}^{2.24}$ and $E = 12.07 \times \rho_{ash}^{1.18}$, and the bounds of ε_3 were determined by $E = 10.22 \times \rho_{ash}^{1.18}$ and $E = 12.07 \times \rho_{ash}^{2.24}$.

The relative percentage differences (defined as the difference between the maximal and minimal values divided by the minimal value) of these mechanical parameters across the tibial VOI are shown in Fig. 5. The relative percentage differences of ε_1, ε_3, and SED ranged from 8% to 28%, from 20% to 28%, and from 14% to 21%, respectively (Fig. 5).

4. Discussion

The purpose of this study is to evaluate the effect of uncertainty in bone material property on the mechanical environment of the bone using heterogeneous FE models and stochastic analysis. This study aims to provide guidelines on the adoption of bone density-modulus relationship in heterogeneous FE models.

Two major findings were revealed from this study. First, we found that if the softest bone model was used instead of the
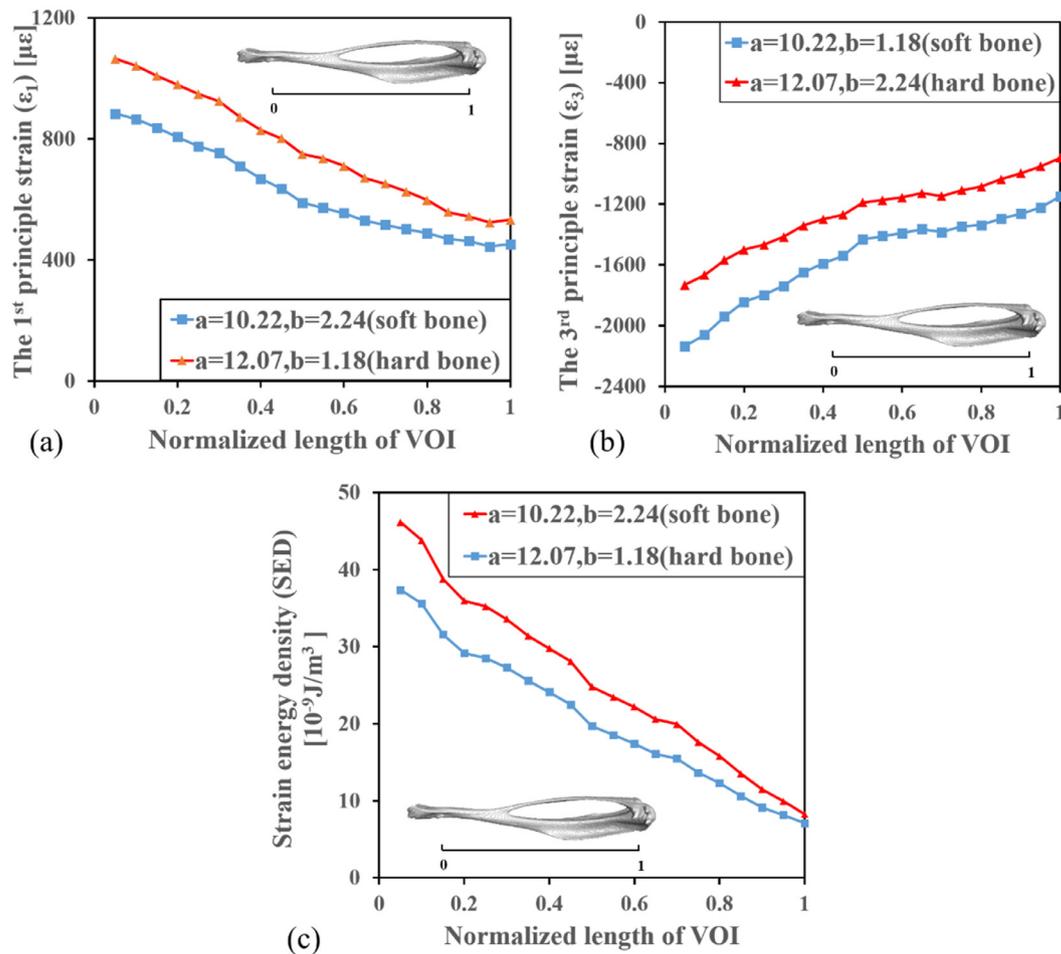
Fig. 4. The material uncertainty-induced bounds of the 1st principal strain, the 3rd principal strain, and the strain energy density across the tibial volume of interest (VOI), with the corresponding density-modulus relationships. The dotted data are the mean values in the 20 compartments across the tibial VOI.

hardest bone model, 3% occurrence of ε_1 were shifted above 250 με, and 5% occurrence of ε_3 were shifted below -250 με. This affects the study of the bone mechano-regulation mechanism, which was first proposed by Wolff and Frost [27,28]. In particular, Frost's mechano-regulation theory suggests that the local bone mass increases when the strain is above a certain upper strain threshold, and decreases when the strain is below a certain lower strain threshold [27]. Furthermore, it has been postulated that the local bone mass is not responsive of the strain when it is within the interval encompassed by these lower and upper thresholds, i.e., the "lazy zone" [29]. If -250 με and 250 με were set as the lower and upper bounds of the "lazy zone" [30], respectively, this study implies that approximately 8% ($=3\% + 5\%$) of the bone voxels will become inactive in the bone adaptation process if the hardest bone model, instead of the softest model, was used in the heterogeneous FE models. Therefore, the uncertainty in bone material property affects the quantification of mechanical stimulation signals of the bone, and is crucial in the study of the bone mechano-regulation mechanism. Next, we found that owing to the uncertainty in bone material property, the mechanical environment across the mouse tibial VOI was changed by up to 28%, 28%, and 21% for ε_1, ε_3 and SED, respectively, thereby indicating the importance of assigning the appropriate bone properties in studies such as the FE validation study. We also found that the bone mechanical environment (ε_1, ε_3, and SED) and the bone density-modulus relationship exhibited the same change trend. Therefore, using the bone density-modulus relationship consistently for defining the bone property could be a feasible strategy in parametric studies, such as evalu-

ating the effect of medicine intervention on the bone mechanical behavior [10].

It is noteworthy that in the present study, the magnitude of the load applied is 11 N [7] to engender 1200 με at the medial midshaft of the tibia [31], and thus elicit an osteogenic response in the mouse tibia [32]. Next, the bone density-modulus relationships available in the literature are subject-specific and site-specific [33] because the bone density-modulus relationships are derived from the mechanical testing of organ-level specimens (e.g., vertebra) in previous studies [34,35]. Hence, a universal deterministic bone density-modulus relationship is required that poses a significant challenge for future research. The universal relationship might be achieved by the investigations at the bone tissue (microstructural) level. Once the tissue-level relationship is developed, the accuracy of heterogeneous μFE models will be increased significantly, because the mapping from bone density to modulus is defined at the bone-tissue level in the heterogeneous μFE models. Furthermore, in the present study, ε_1, ε_3, and SED were selected to describe the bone mechanical environment, because ε_1 is likely to be linked to the mode I (opening) bone fracture, ε_3 is the compressive strain reflecting the loading scenario performed in this study, and SED is the resultant bone parameter containing information of both strain and stress that is highly correlated with bone adaptations [20]. Additionally, a limitation in the present study is that the FE analysis was only performed under the loading of axial compression. Other complex loading scenarios, such as the three-point bending, are not investigated. However, because axial compression was used widely in previous preclinical studies of bone adaptations
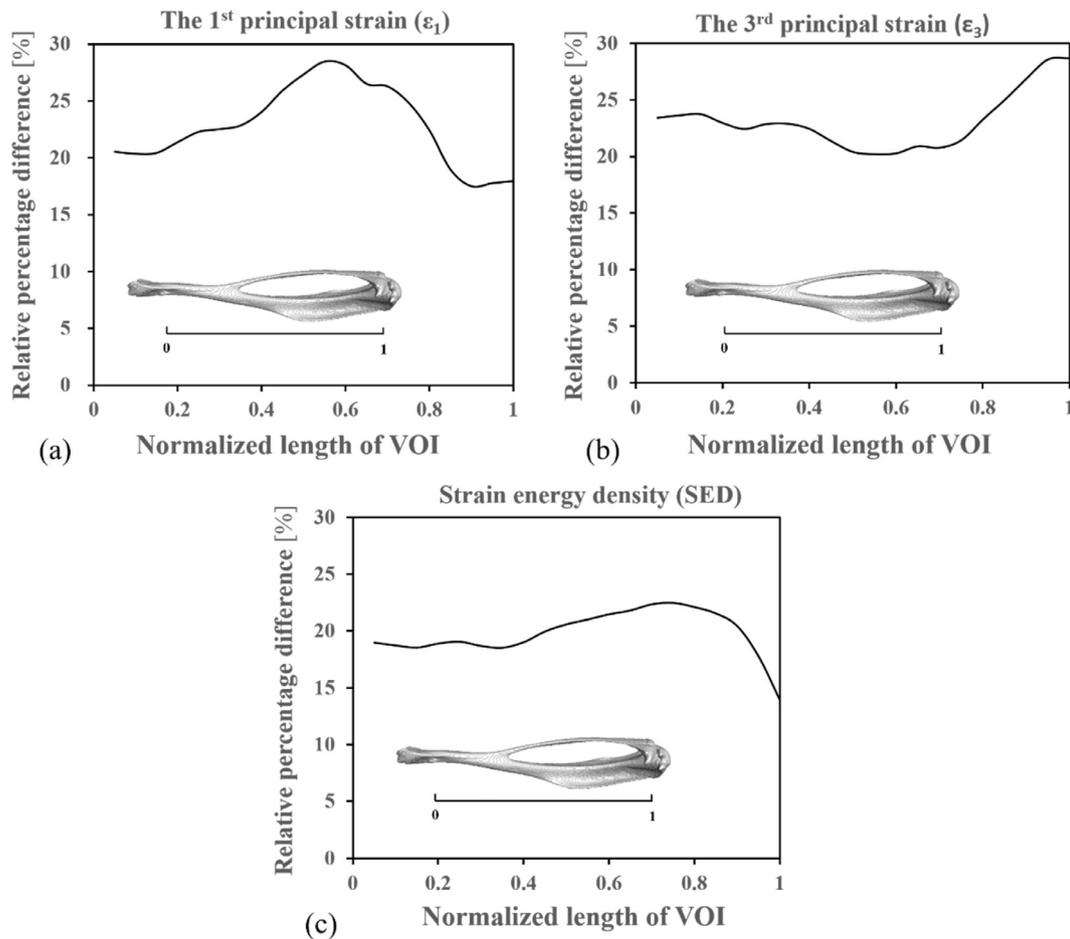
Fig. 5. The relative percentage differences of tibial mechanical parameters across the tibial volume of interest (VOI). Data are presented as the differences between the maximal and minimal values divided by the minimal values in the 20 compartments across the tibial VOI.

[7,10], the results from this study can be referred easily for a comparison.

In summary, uncertainty in the bone material property exhibited a marked effect on the mechanical environment of the bone, thus implying that the bone density-modulus relationship should be assigned appropriately in studies such as the investigation of the bone mechano-regulation mechanism and FE validation. However, the change trend in the bone mechanical environment is consistent with that of the bone density-modulus relationship, thus suggesting that assigning bone density-modulus relationships in the FE models consistently could be feasible for parametric studies. This study provides guidelines on the adoption of the bone density-modulus relationship in heterogeneous FE models.

Conflict of interest

The authors declare that there is no conflict of interest.

Funding

References

[1] Bouxsein ML, Boyd SK, Christiansen BA, Guldberg RE, Jepsen KJ, Mueller R. Guidelines for assessment of bone microstructure in rodents using micro-computed tomography. J Bone Miner Res 2010;25(7):1468–86.

[2] Lukas C, Ruffoni D, Lambers FM, Schulte FA, Kuhn G, Kollmannsberger P, Weinkamer R, Mueller R. Mineralization kinetics in murine trabecular bone quantified by time-lapsed in vivo micro-computed tomography. Bone 2013;56:55–60.

[3] de Bakker CM, Altman AR, Tseng WJ, Tribble MB, Li C, Chandra A, Qin L, Liu XS. μCT-based in vivo dynamic bone histomorphometry allows 3D evaluation of the early responses of bone resorption and formation to PTH and alendronate combination therapy. Bone 2015;73:198–207.

[4] Lambers FM, Kuhn G, Weiqt C, Koch KM, Schulte FA, Mueller R. Bone adaptation to cyclic loading in murine caudal vertebrae is maintained with age and directly correlated to the local micromechanical environment. J Biomech 2015;48:1179–87.

[5] Lu Y, Boudiffa M, Dall'Ara E, Liu Y, Bellantuono I, Viceconti M. Longitudinal effects of parathyroid hormone treatment on morphological, densitometric and mechanical properties of mouse tibia. J Mech Behav Biomed Mater 2017;75:244–51.

[6] Patel TK, Brodt MD, Silva MJ. Experimental and finite element analysis of strains induced by axial tibial compression in young-adult and old female C57Bl/6 mice. J Biomech 2014;47:451–7.

[7] Razi H, Birkhold AI, Zaslansky P, Weinkamer R, Duda GN, Willie BM, Checa S. Skeletal maturity leads to a reduction in the strain magnitudes induced within the bone: a murine tibia study. Acta Biomater 2015;13:301–10.

[8] Willie BM, Birkhold AI, Razi H, Thiele T, Aido M, Kruck B, Schill A, Checa S, Main RP, Duda GN. Diminished response to in vivo mechanical loading in trabecular and not cortical bone in adulthood of female C57Bl/6 mice coincides with a reduction in deformation to load. Bone 2013;55:335–46.

[9] Easley SK, Jekir MG, Burghardt AJ, Li M, Keaveny TM. Contribution of the intra-specimen variations in tissue mineralization to PTH- and raloxifene-induced changes in hardness of rat vertebrae. Bone 2009;46:1162–9.

[10] Wang N, Rumney RM, Yang L, Robaye B, Boeynaems JM, Skerry TM, Gartland A. The P2Y13 receptor regulates extracellular ATP metabolism and the osteogenic response to mechanical loading. J Bone Miner Res 2012;28(6):1446–56.

[11] Yang H, Butz KD, Duffy D, Niebur GL, Nauman EA, Main RP. Characterization of cancellous and cortical bone strain in the in vivo mouse tibial loading model using microCT-based finite element analysis. Bone 2014;66:131–9.

[12] Lu Y, Engelke K, Glueer CC, Morlock MM, Huber G. The effect of in situ/in vitro three-dimensional quantitative computed tomography image voxel size on the finite element model of human vertebral cancellous bone. Proc Inst Mech Eng H 2014;228(11):1208–13.

[13] Helgason B, Perilli E, Schileo E, Taddei F, Brynjofsson S, Viceconti M. Mathematical relationships between bone density and mechanical properties: a literature review. Clin Biomech 2008;23(2):135–46.

[14] Knowles NK, Reeves JM, Ferreira LM. Quantitative computed tomography derived bone mineral density in finite element studies: a review of the literature. J Exp Orthoped 2016;3:36–52.

[15] Costa MC, Tozzi G, Cristofolini L, Danesi V, Viceconti M, Dall'Ara E. Micro finite element models of the vertebral body: validation of local displacement predictions. PLoS One 2017;12(7):e0180151.

[16] Levchuk A, Zwahlen A, Weiqt C, Lambers FM, Badilatti SD, Schulte FA, Kuhn G, Mueller R. Large scale simulations of trabecular bone adaptation to loading and treatment. Clin Biomech 2014;29:355–62.

[17] Webster D, Wirth A, van Lenthe GH, Mueller R. Experimental and finite element analysis of the mouse caudal vertebrae loading model: prediction of cortical and trabecular bone adaptation. Biomech Model Mechanobiol 2012;11:221–30.

[18] Berthaume MA, Dechow PC, Iriarte-Diaz J, Ross CF, Strait DS, Wang Q, Grosse IR. Probabilistic finite element analysis of a craniofacial finite element model. J Theor Biol 2012;300:242–53.

[19] Laz PJ, Stowe JQ, Baldwin MA, Petrella AJ, Rullkoetter PJ. Incorporating uncertainty in mechanical properties for finite element-based evaluation of bone mechanics. J Biomech 2007;40:2831–6.

[20] Taddei F, Martelli S, Reggiani B, Cristofolini L, Viceconti M. Finite element modeling of bones from CT data: sensitivity to geometry and material uncertainties. IEEE Trans Biomed Eng 2006;53:2194–200.

[21] Wille H, Rank E, Yosibash Z. Prediction of the mechanical response of the femur with uncertain elastic properties. J Biomech 2012;45:1140–8.

[22] Lu Y, Boudiffa M, Dall'Ara BellantuonoI, Viceconti M. Development of a protocol to quantify local bone adaptation over space and time: quantification of reproducibility. J Biomech 2016;49:2095–9.

[23] Turkowski K, Gabriel S. Filters for common resampling tasks. In: Glassner AS, editor. Graphics gems 1. Academic Press; 1990. p. 147–65.

[24] Keller TS. Predicting the compressive mechanical behavior of bone. J Biomech 1994;27:1159–68.

[25] Cerdà V, Cerdà JL, Idris AM. Optimization using the gradient and simplex methods. Talanta 2016;148:641–8.

[26] Hanss M, Klimke A. On the reliability of the influence measure in the transformation method of fuzzy arithmetic. Fuzzy Set Syst 2004;143:371–90.

[27] Frost HM. Bone's mechanostat: a 2003 update. Anat Rec A Discov Mol Cell Evol Biol 2003;275:1081–101.

[28] Wolff J. Concerning the interrelationship between form and function of the individual parts of the organism. Clin Orthop Relat Res 1988;228:2–11.

[29] Beaupre GS, Orr TE, Carter DR. An approach for time-dependent bone modeling and remodeling application: a preliminary remodeling simulation. J Orthop Res 1990;8:662–70.

[30] Geraldes DM, Phillips AT. A comparative study of orthotropic and isotropic bone adaptation in the femur. Int J Numer Method Biomed Eng 2014;30:873–89.

[31] Fritton JC, Myers ER, Wright TM, van der Meulen MC. Loading induced site-specific increases in mineral content assessed by microcomputed tomography of the mouse tibia. Bone 2005;36:1030–8.

[32] Sugiyama T, Saxon LK, Zaman G, Moustafa A, Sunters A, Price JS, Lanyon LE. Mechanical loading enhances the anabolic effects of intermittent parathyroid hormone (1-34) on trabecular and cortical bone in mice. Bone 2008;43:238–48.

[33] Eberle S, Göttlinger M, Augat P. An investigation to determine if a single validated density-elasticity relationship can be used for subject specific finite element analyses of human long bones. Med Eng Phys 2013;35:875–83.

[34] Morgan EF, Bayraktar HH, Keaveny TM. Trabecular bone modulus-density relationships depend on anatomic site. J Biomech 2003;36:897–904.

[35] Schileo E, Dall'Ara E, Taddei F, Malandrino A, Schotkamp T, Baleani M, Viceconti M. An accurate estimation of bone density improves the accuracy of subject-specific finite element models. J Biomech 2008;41:2486–91.